Materials Chemistry and Physics 313 (2024) 128710

Contents lists available at ScienceDirect

Materials Chemistry and Physics

journal homepage: www.elsevier.com/locate/matchemphys

Increased NIR photoluminescence of Egyptian blue via matrix effect optimization

Marco Nicola [a,b,*], Claudio Garino [a], Sophia Mittman [c], Emanuele Priola [a], Luca Palin [d,e], Marta Ghirardello [f], Vamshi Damagatla [f], Austin Nevin [g], Admir Masic [c], Daniela Comelli [f,**], Roberto Gobetto [a]

[a] Dipartimento di Chimica, Università degli Studi di Torino, Via Giuria, 7, 10125, Torino, Italy
[b] Adamantio srl, Science in Conservation, Via Napione, 29/A, 10124, Torino, Italy
[c] Department of Civil and Environmental Engineering, Massachusetts Institute of Technology, Cambridge, MA, 02139, USA
[d] Dipartimento di Scienze e Innovazione Tecnologica, Università del Piemonte Orientale, Via T. Michel 11, 15121, Alessandria, Italy
[e] Nova Res s.r.l., Via D. Bello 3, 28100, Novara, Italy
[f] Dipartimento di Fisica, Politecnico di Milano, Piazza Leonardo da Vinci, 32, 20133, Milano, Italy
[g] Courtauld Institute of Art, Somerset House, London, WC2R 0RN, UK

HIGHLIGHTS

- We report solid-state synthesis of cuprorivaite starting from silica nanoparticles.
- The synthetized material displays an exceptionally high quantum yield ($\Phi_{EM} \approx 30$ %).
- The synthesized tiny crystals are almost devoid of any copper-rich glassy phase.
- We demonstrate how limiting the glassy phase increases the external quantum efficiency.
- The results can greatly boost the use of cuprorivaite in energy saving and biomedicine.

ARTICLE INFO

Keywords:
Egyptian blue
Cuprorivaite
NIR photoluminescence
Quantum yield
Silica nanoparticles
Solid-state synthesis
Melt-flux synthesis

ABSTRACT

The exceptionally high NIR photoluminescence of the ancient pigment Egyptian blue is due to its very stable phase cuprorivaite ($CaCuSi_4O_{10}$). This compound has recently attracted significant attention, leading to numerous applications for sensors, luminescent solar concentrators, energy-saving, and biomedicine. Here we report an innovative manufacturing process for producing high-grade cuprorivaite, characterized by fine crystal grains and a significantly increased NIR photoluminescence emission. The unprecedented ultra-high NIR emission (quantum yield $\Phi_{EM} \approx 30$ %) is almost three times higher than the best one reported so far. This is an important turning point for the extension of applications of cuprorivaite to new sectors and can greatly boost its exploitation. The new high-efficiency cuprorivaite is obtained by solid-state synthesis, using silica nanoparticles as a starting material and avoiding fluxing agents. No doping with rare-earths or other elements has been employed, making synthesis straightforward and sustainable. The material obtained has been fully characterized in terms of crystalline, morphological, and optical properties and compared to cuprorivaite obtained through traditional melt-flux synthesis. The main difference observed is that the tiny crystals obtained through the new synthesis method are practically devoid of the glassy phase, rich in copper and impurities, that is instead largely present in Egyptian Blue pigment synthesized with traditional melt-flux synthesis. We speculate that this glassy phase is responsible for the partial suppression of the intrinsic photoluminescence of cuprorivaite, demonstrating how limiting the glassy phase can increase the external quantum efficiency of Egyptian blue.

* Corresponding author. Dipartimento di Chimica, Università degli Studi di Torino, Via Giuria, 7, 10125, Torino, Italy.
** Corresponding author.
E-mail addresses: nicola@adamantionet.com (M. Nicola), daniela.comelli@polimi.it (D. Comelli).

https://doi.org/10.1016/j.matchemphys.2023.128710
Received 17 September 2023; Received in revised form 14 November 2023; Accepted 21 November 2023
Available online 3 December 2023

1. Introduction

One of the main goals of modern materials science is to prevent looming supply crises and health or environmental risks. This aim can be achieved by replacing strategic products from rare or dangerous sources with high-performance, naturally abundant, safe and suitable materials.

Help can come from newly discovered properties of traditional and commonplace materials. A well-known case is the exploitation of graphite and the synthesis of graphene that has been harnessed to address extraordinary applications. Many other promising substances with unique photonic properties have been studied with this purpose and are under evaluation, among them is the ancient pigment Egyptian Blue (EB).

EB is a bright blue inorganic pigment mainly constituted by sub-millimeter crystals of $CaCuSi_4O_{10}$. It is extremely stable [1] under a very wide range of temperature, pH, oxygen content and light irradiation and since it is made up of abundant, safe and inexpensive elements, it has a great potential as substitute of less sustainable or problematic modern blue pigments [2]. However, in addition to its color, EB has recently attracted high and growing interest for its functional characteristics [3] i.e. antibacterial, angiogenic, and osteogenic activity [4,5], and most notably, high NIR reflectance [6] and outstanding NIR photoluminescence (PL) [7].

Already produced more than 5000 years ago [8], EB is considered the first synthetic blue pigment [1,9]. It was the most popular blue in the classical era [6] but the secret of its synthesis was lost during the Middle Ages [2]. A method to produce EB was fully recovered only in the late 19th century, following efforts of Chaptal [10] and Davy [11]. During the 1900s, EB was primarily studied within archeology and by scientists evaluating its mineralogical and crystallographic properties [7,8,12]. The use of EB as a modern blue pigment was also attempted [13], but found only limited success, mainly due to the difficulty of obtaining a fine bright blue thin powder after the production via melt-flux that *de facto* was the only available route of synthesis [14,15].

At the end of the millennium, an intriguing technological breakthrough was triggered by the discovery of the exceptional NIR PL of EB and related materials, which can be induced by NIR, and visible light [8], as well as UV [16]. Starting from archaeometry studies [9], this feature has been exploited in an increasingly wide range of applications spanning the fields of sensors [17], energy saving (i.e. "cool" pigments) [2,18–20], phosphors [21], forensic science [22], and luminescent solar concentrators [23]. In 2013, the development of a method to exfoliate EB and produce 2D photoluminescent nano-sheets [24] further increased the interest in the pigment, expanding the family of 2D materials [25–27]. This newly discovered feature opened the way to applications in next-generation fields such as security inks [28,29] and especially biological imaging and biomedicine [5,30–33].

EB owes its blue color to Cu^{2+} ions in square-planar coordination [34]. This chromogenic unit is contained within the main constituent of EB, namely crystalline $CaCuSi_4O_{10}$, a compound also commonly referred to as cuprorivaite i.e. the rare natural mineral with same composition and structure [35]. Cuprorivaite is a phyllosilicate within the family of gillespite ($BaFeSi_4O_{10}$), tetragonal space group *P4/ncc* [36]. It is isostructural with the closely related mineral effenbergerite ($BaCuSi_4O_{10}$ – the main constituent of the ancient pigment Chinese blue) and wesselsite ($SrCuSi_4O_{10}$) [36,37], both showing color and photoluminescence properties similar to EB [8,18]. It is noted that apart from cuprorivaite, EB commonly contains unreacted silica, other calcium and copper compounds and overall, an amorphous glassy phase rich in copper and impurities [38]. Indeed, the presence of a relatively extended glassy matrix is peculiar in EB produced using melt-flux production techniques. These methods are the most popular manufacturing techniques for producing EB, and similar methods were also used in antiquity. Melt-flux methods (also reported as salt-flux syntheses) imply the use of a flux (e.g. soda or plant ash) that lowers the melting point of silica, allowing the production of cuprorivaite in the 800–900 °C temperature range [15,24].

Cuprorivaite can also be produced through a direct solid-state synthesis without the use of any flux, by raising the temperature to about 1000 °C [24,39,40]. In this case the main processes involved can be considered surface diffusion of Ca and Cu ions on the surface of silica particles [38,41]. Overall, this second method almost completely avoids the formation of a glassy matrix [38,41], but it is not very efficient, as the production of cuprorivaite is limited to the surface of the starting silica grains [42,43]. Recently, cuprorivaite has been produced through other methods such as hydrothermal synthesis [44], solution combustion synthesis [45], sol-gel synthesis [2,4,46], and pseudomorphosis [47]. However, the impact of the route of synthesis on the PL quantum yield has not yet been properly discussed.

In general, cuprorivaite shows an intense PL between 910 and 918 nm, with a lifetime ranging from 100 μs to 140 μs[7,21,49,55]. This emission is associated with the electronic transition $^2B_{2g} \rightarrow {}^2B_{1g}$, centered on Cu^{2+} complex ions in a D_{4h} symmetry, and is stimulated by a broadband absorption at 630 nm ($^2B_{1g} \rightarrow {}^2E_g$), with other important bands at about 780 nm[48] ($^2B_{1g} \rightarrow {}^2B_{2g}$) and 536 nm ($^2B_{1g} \rightarrow {}^2A_{1g}$) [21]. Recently, it has been demonstrated that EB absorbs also in the UV [16].

In 2009, Accorsi et al. [7] determined the exceptional PL quantum yield of a commercially available EB (i.e. Kremer Pigmente) as $\Phi_{EM} = 10.5$ %, while, very recently, Rajaramanan et al. have reported the production of EB powders via melt-flux synthesis with a slightly higher quantum yield ($\Phi_{EM} = 12.9$ %) [49]. The research by Accorsi [7] paved the way to the modern exploitation of EB. In the following years, attempts to produce cuprorivaite with improved NIR optical properties and PL emission have been carried out, especially for applications as a cool pigment. Variously substituted cuprorivaite and doping with rare-earth elements were tested to reduce the NIR self-absorption and improve the NIR solar reflectance [2,20,46,50]. In 2018, Bredhal et al. [18] concluded that an accurate wash with HCl can remove CuO impurities from commercial EB, improving the PL efficiency. The effect of the glassy matrix and of the route of synthesis were suggested by Nicola et al., in 2019 [42,51], showing an increase in PL of EB obtained by conventional solid-state synthesis in comparison to that obtained by melt-flux synthesis, leading to the hypothesis that the Cu-containing glass-matrix could be responsible for the partial suppression of the PL, but no definitive conclusions were drawn, nor was a route of synthesis to minimize this effect defined. Recently, the emission enhancement of EB mixed with gold nanoparticles was investigated, demonstrating a 4-fold increase in emission intensity of EB intrinsic photoluminescence [52].

As previously quoted, the production of cuprorivaite implies a heat treatment at a temperature ranging from 350 °C (hydrothermal synthesis [44]) to 850–1100 °C [1,4,24,47]. The amount of amorphous phase strongly depends on this temperature value as well as on the cooling rate, which is often poorly described. The result achieved varies and even standardized procedures proposed are not able to achieve a homogeneous result since the dimension of silica grains, and other key parameters, are seldom or very poorly specified. Indeed, synthesis methods generally overlook arbitrary parameters (e.g. how long and how intensively reagents are ground) and produce variation in particle sizes (e.g. grain size of 5–20 μm after manual grinding) [24]. The grinding procedure of the product obtained is another key passage that is often overlooked. Indeed, as is observed with phosphors, grinding can heavily affect the luminescence output of EB [1,53] and thus the effect of manual grinding (i.e. the common procedure adopted by all authors) on the properties of the produced EB material should be carefully considered.

In this work, we present the production of EB with an unprecedented quantum yield of almost 300 % higher (Φ_{EM} about 30.0 %) than the best one reported so far [49], using an improved solid-state synthesis starting from silica nanoparticles. In the following, we provide details on the employed synthesis method as well the characterization of the newly synthesized EB powders in terms of morphological, crystalline, and optical properties, comparing it to cuprorivaite particles and

commercially available EB pigments, all produced through traditional melt-flux synthesis.

We remark here that a true cuprorivaite standard does not exist. Indeed, few manufacturers produce and sell EB (e.g. Kremer Pigmente and Natural Pigments) [15] and the vast majority of papers dealing with cuprorivaite have employed these pigments as the cuprorivaite reference [7–9,17,18,23,31,47,49,54–58]. Instead, pure crystalline artificial cuprorivaite is not commercially available. Even the self-production of pure cuprorivaite is not a feasible way for its supply, since all synthesis routes invariably yield impure crystalline cuprorivaite [24] with the presence of extraneous and undesired compounds, such as silica [44] (i.e. unreacted silica or silica polymorphs) and often also CuO or $CaSiO_3^1$. It is noted that XRPD analysis commonly used to assess the purity of self-made cuprorivaite [21,39] is not a fully reliable method since, in general, it is not able to quantify the amount of the amorphous glassy phase present, unless Rietveld refinement is used. Hence, while in this paper we used different types of cuprorivaite as references, we point out that the search for purer and more homogeneous standards for cuprorivaite remains an important challenge that should be addressed in the close future.

2. Methods

2.1. Materials for synthesis

The chemical reagents used, $CuCO_3{\cdot}Cu(OH)_2$ (reagent grade), $CaCO_3$ (purity ≥99.0 %), and Na_2CO_3 (purity ≥99.0 %), were purchased by Sigma-Aldrich. The regular silica source is pumice powder, 60–65 μm supplied by Chimica Strola, Torino. The silica nanoparticles used are from amorphous colloidal silicon dioxide (i.e. pyrogenic silica or fumed silica), manufactured by Evonik and commercialized as AEROSIL200 (according to the producer SiO_2 purity ≥99.8 %, average particle size 12 nm). Prior to the synthesis, silica sources were tested with SEM-EDS to check for detectable impurities (e.g., K and Al) that can play a role in the production process. They resulted with concentrations of those specimens below the detection limit.

2.2. Reference commercial samples

Two commercial samples of EB have been purchased from Kremer Pigmente, and here are referred to as K120 and K10. According to the manufacturer, K120 (Kremer Pigmente item #10060) has pigment grains less than 120 μm in diameter, while K10 (Kremer Pigmente item #100601, no longer commercially available) has smaller pigment grains (diameter up to 10 μm) obtained through mechanical grinding of the powder after synthesis. Although Kremer Pigmente does not provide any information on the synthesis method used for its EB pigments, it is highly likely to have been synthesized by a traditional melt-flux method.

2.3. Structural characterization methods

A Hitachi FLEXSEM 1000 was used for electron microscopy observation. A tungsten filament was used as the electron source at 15 kV. SEM-EDS data were instead collected on resin-embedded samples using a TESCAN RISE scanning electron microscope. All samples were imaged in a low vacuum (30 Pa) with an acceleration voltage of 20 keV (air type: N2). Acquisition time for EDS data was 12 h. EDS data were quantified using Bruker Esprit 2.1 Software with 2 × 2 data binning and Linemarker PB-ZAF correction. SEM-EDS data were further processed using custom MATLAB (R2019a) scripts.

XRPD data were collected with a Bruker D8 Advance diffractometer, equipped with a copper X-ray source and a LynxEye XE-T detector. The measurement conditions of the source were set at 40 mA and 40 kV. The radius of the goniometer was set in the standard measurement conditions at 280 mm. For the determination of the amorphous content the internal standard material chosen was a commercial rutile produced by DuPont known as R900 [59]. Rietveld refinements were performed using Topas Academic V.7[60,61].

2.4. Optical characterization methods

PL emission spectra and quantum yields were acquired with a HORIBA Scientific Fluorolog spectrofluorometer, equipped with a 450 W Xenon lamp, and two detectors: a Hamamatsu R928 photomultiplier for the measurements in the visible range (sensitivity spectral range 290–850 nm) and a liquid nitrogen cooled InGaAs photodiode for measurements in the NIR region (sensitivity spectral range 850–1600 nm). The liquid nitrogen cooled InGaAs photodiode was used to acquire the emission of Egyptian blue in the NIR region, while the R928 was employed to evaluate the absorption of the exciting light at 630 nm. The signals, corrected for the spectral efficiency of the corresponding detector, were used to evaluate the absolute QY. For this latter measurement the spectrofluorometer was equipped with a Quanta-φ integrating sphere.

The PL decay kinetic from samples, placed as powder dispersions over a thin silica slide, was excited by nanosecond Q-switched laser pulses at 532 nm (FTSS 355-50 Crylas GmbH), and detected by a time-gated intensified camera (C9546-03, Hamamatsu Photonics) [62] equipped with a longpass filter with its transmission edge at 800 nm. The detector gating window was set to 50 μs and the decay kinetic was recorded through the collection of a series of time-gated images delayed from 1 to 750 μs from laser pulses. The temporal decay of the total intensity of the emission in the spectral band 800–890 nm was fitted with a mono-exponential decay to retrieve the average emission lifetime of each sample. Repeatability measurements on different points of the same sample have inferred a lifetime precision of 0.9 μs.

The PL self-absorption of samples was studied through time-domain diffuse optical spectroscopy. The system, fully described elsewhere [63], consists of a pulsed picosecond light source (fiber based supercontinuum, SuperK Extreme, NKT photonics), a Time-Correlated Single Photon Counting (TCSPC) detection system, and a fiber based optical path to deliver and collect the light from the sample. The powder sample, mixed with NaCl (Sigma Aldrich, ≥99.5 %) in a ratio of 1:100 (sample:salt), is placed in a black cylindrical holder (Ø 2.5 cm and height of about 1.3 cm). The light is injected into the sample and the diffuse light exiting from the opposite side of the cylinder is collected by an optical fiber. The wavelength of the injection light is scanned over the spectral range of 600–1100 nm in steps of 10 nm and time-resolved measurements are performed at each injected wavelength. Data analysis consists in fitting, for each injection wavelength, the distributed time-of-flight (DTOF) curve of the light transmitted by the sample with the analytical solution of the diffusion approximation of the radiative transport equation and applying the Extrapolated Boundary conditions to recover the optical absorption coefficient at each wavelength.

3. Results

3.1. Preparation of cuprorivaite powders

The $CaCuSi_4O_{10}$ powders were produced in a ceramic kiln WLF 2000 Light & Power regulated by a Pixsys ATR243 controller. As proposed by Warner [31] and Mazzocchin et al. [58], the syntheses were carried out in self-made terracotta crucibles. The clay used to produce the terracotta crucibles was purchased from Colorobbia and was of the quality "Argilla Raku Bianca Fine". Prior to the syntheses, the crucibles were heated at 1000 °C for 12 h and naturally cooled down to 20 °C. Subsequently they were washed in deionized water and naturally dried.

Two different methods of synthesis were used (Fig. 1):

(i) The first one, overall referred to as "traditional synthesis" or "melt-flux method", implies a mainly melt-flux dynamic and was

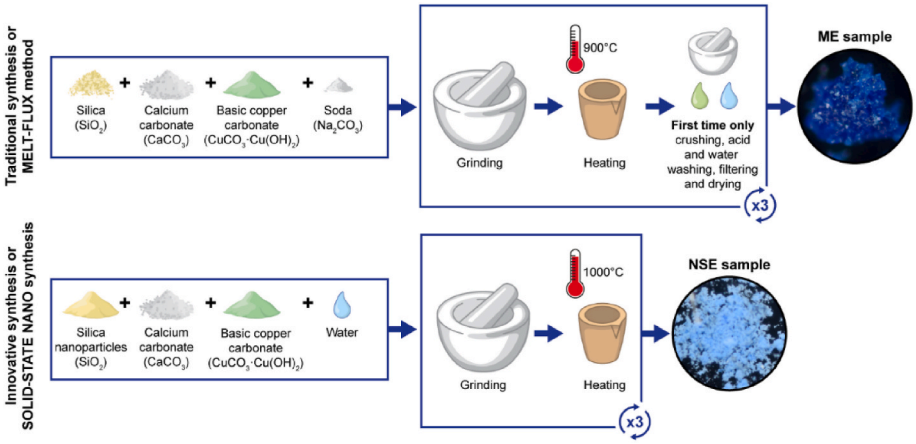

Fig. 1. Schematic view of the synthesis method employed to produce ME and NSE samples.

employed to produce the sample in the following referred to as ME.

(ii) The second one is referred to as "innovative synthesis" or "solid-state nano synthesis" and implies an almost complete solid-state reaction [21] occurring on silica nanoparticles. This second method was used to produce the NSE sample.

The ME sample was produced by mixing the reagents in stoichiometric ratios and adding approximately 8 % w/w Na_2CO_3 as a fluxing agent and approximately 5 % w/w of extra silica to counteract the excess of Na. The respective reactants were finely ground and mixed in a ceramic mortar then placed in a terracotta crucible and heated. The mixture was initially heated at a rate of 2 °C/min until 900 °C and then held at that temperature for 12 h. At the end, the temperature was cooled down to 20 °C with a cooling rate of 2 °C/min. Once at room temperature, the solidified blue-blackish mass was removed from the crucible and was crushed. Later, as suggested in the literature [8,21], the sample was washed to remove some poorly reacted material (e.g. CuO), by soaking it in 50 mL of 1 M HCl for 48 h. Afterward, the powder was washed with 50 mL of distilled water and was filtered and dried. Two analogous cycles of reheating and crushing were then performed to improve the quality of the final product which presented a bright deep blue tone.

The NSE sample was produced using the AEROSIL200 silica nanoparticles instead of regular silica and avoiding the use of fluxing agents. The other reactants were finely ground in a ceramic mortar and then added to the silica in stoichiometric ratios. 10 mL of distilled water was added for each gram of nanosilica used to obtain a soft gel. The gel was further mixed and then placed in the crucible. The gel was initially heated at a rate of 2 °C/min until 1000 °C and then held at that temperature for 12 h. At the end, the temperature was cooled down to 20 °C at a cooling rate of 2 °C/min. Once at room temperature, the bright light blue powdery mass was removed from the crucible and easily finely pulverized with a soft touch in the mortar. Afterward, without any washing, it was subjected to two similar cycles of reheating and crushing, to improve the quality of the final product.

To assess the importance of using silica nanoparticles as the starting materials, a further sample, quoted as SE sample, was produced: this sample was obtained through solid-state synthesis (same conditions as NSE) but using regular silica (grains size of 60–65 μm), instead of silica nanoparticles as the starting material.

Finally, two commercial samples of EB purchased from Kremer Pigmente, referred to as K120 and K10 (details in the Methods section), were analyzed as references.

The full list of analyzed samples, which include both reference commercial pigments and synthesized pigments, is provided in Table 1, while in Supporting Information, Fig. S1, the color picture of each sample is provided.

Table 1
List of the analyzed samples reporting information on the synthesis method employed for each sample and its visual appearance. The latter is provided through the calibrated color image of each sample observed under an optical microscope. Details of the employed microscope set-up and full images of samples are provided in Supporting Information Figure S1.

Sample	Provenience	Synthesis	Calibrated color picture
ME	In-house synthesized cuprorivaite powder	Traditional melt-flux method	
NSE	In-house synthesized cuprorivaite powder	Solid-state synthesis from nanosilica	
SE	In-house synthesized cuprorivaite powder	Solid-state synthesis	
K120	Reference commercial sample	Traditional melt-flux method[a]	
K10	Reference commercial sample	Traditional melt-flux method[a] + mechanical grinding	

[a] The pigment producer (Kremer Pigmente) does not provide any information on the synthesis method, but, considering the available industrial manufacturing methods, it is highly likely that sample K120 and K10 have been synthesized by a traditional melt-flux method.

3.2. Morphological and crystalline properties

Backscattered SEM images on cross sections of ME, NSE and SE powders (Fig. 2a) reveal net morphological differences in samples. In ME it is evident that the sample is made of large pigment particles mainly composed of a glassy matrix that embeds large crystals of cuprorivaite. Unreacted grains of silica are visible in the middle of some crystals and the remnants of condensation nuclei are also visible. In contrast, in SE sample, synthesized through solid-state synthesis, the cuprorivaite crystals are present as a tiny layer on the surface of micrometer silica grains that remain largely unreacted. In NSE the small size of the silica nanoparticles allows for an almost complete reaction leaving very little unreacted silica.

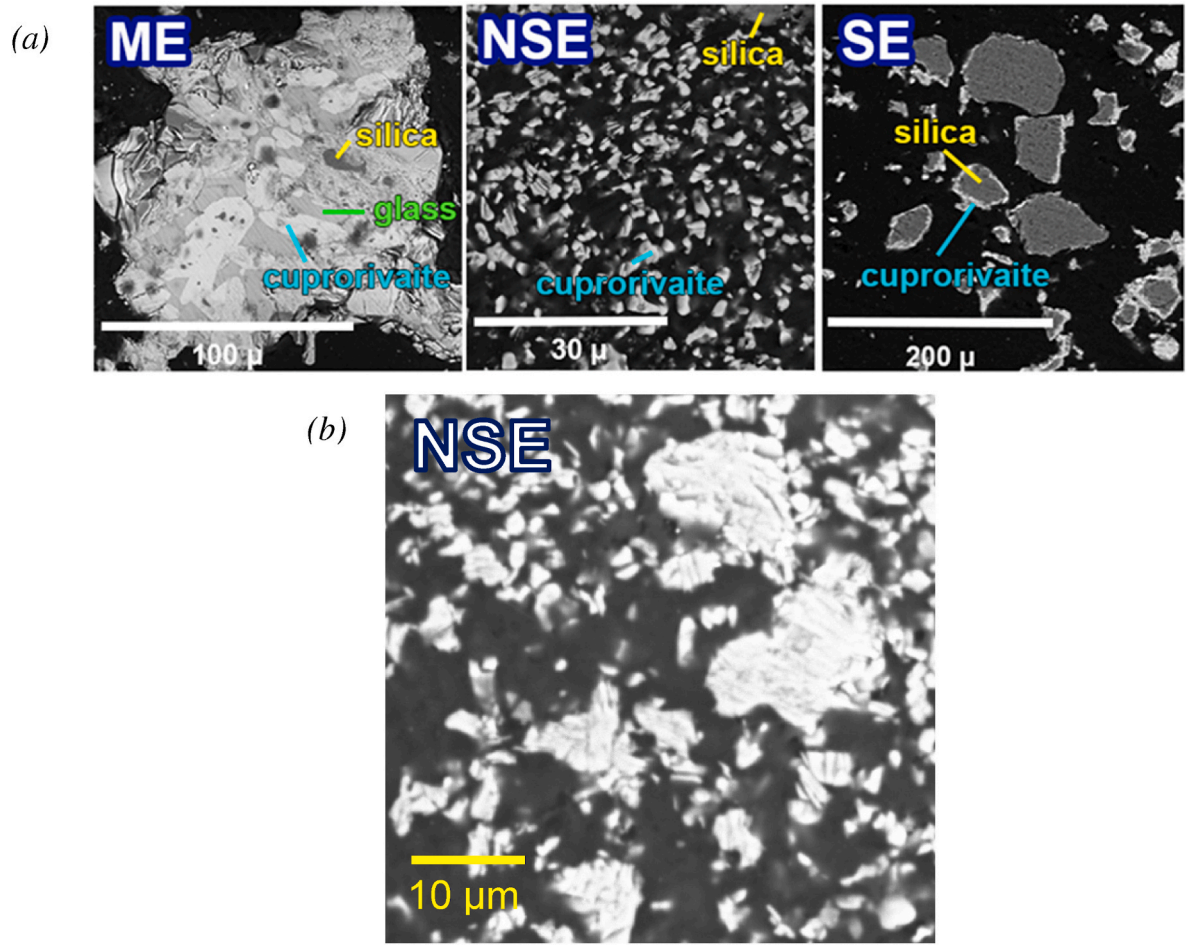

Fig. 2. (a) Backscattered SEM (SEM-BSE) images on cross sections of ME, NSE and SE powders. (b) Lamellar structure of cuprorivaite clearly visible on sample NSE through SEM-BSE image at higher magnification.

It is worth noting that in NSE the characteristic lamellar structure of cuprorivaite is clearly visible (Fig. 2b) and that the dimensions of the particles are much smaller than those observed in ME and SE, even if almost no mechanical grinding has been applied. In fact, NSE particles range in size from a few microns to nanometers, while ME and SE particles are often larger than 50 μm and sometimes exceed 100 μm. Since the NSE sample is strictly superior in comparison with SE in terms of cuprorivaite content, the SE sample is no longer considered in the following of the paper. The SEM analyses on K120 and K10 show the presence of matrices rich in fluxes containing sodium. This confirms that they were obtained through a melt-flux method. Cuprorivaite crystals have a regular morphology in K120, while they appear crushed in K10, suggesting that the latter sample was ground to reduce the size of the pigment grains.

X-ray diffraction data, analyzed through the Rietveld Refinement, demonstrate that the NSE sample has the highest content of crystalline cuprorivaite (around 76 %) and the lowest content of amorphous compounds (22 %), while the other samples, synthetized through the melt-flux method, have an amorphous content always higher than 36 % (Table 2).

By combining XRPD and SEM-EDS analysis (Fig. 3) we finally infer that cuprorivaite is present in all samples. However, cuprorivaite is surrounded by different amounts of an amorphous matrix depending on the sample, the remaining crystalline phases being mainly constituted by very low percentage of silica polymorphs (i.e. quartz, tridymite and cristobalite).

3.3. Optical properties

All the analyzed samples exhibit the same PL spectrum, with a maximum emission around 915 nm (Fig. S2 in Supporting Information) and a microsecond lifetime similar for all the samples (average between samples $< \tau \geq 135 \pm 2$ μs), apart for sample K10, which shows a shorter lifetime, $\tau = 123$ μs (decay kinetics data are provided in Fig. S3 in Supporting Information). Instead, the samples display a strong variability in terms of quantum yield, equal to 29.9 % for NSE and below 11

Table 2
Morphological and crystalline properties of ME, NSE, K10 and K120 samples retrieved through SEM, SEM-EDS and XRPD analyses.

Sample	Pigment particle size [μm] (SEM)	Crystal size and morphology (SEM-BSE)	Cuprorivaite weight % (XRPD)	Amorphous weight % (XRPD)	Silica polymorphs weight % (XRPD)	Glass-matrix distribution (SEM-EDX)
ME	100	Large tabular crystals	55.7	44.3	0.0	widespread
NSE	2–3	Small tabular crystals	76.5	22.1	1.4	trace
K10	7–10	Crushed tabular crystals	61.9	35.7	2.4	limited
K120	80–100	Large tabular crystals	45.1	49.3	5.6	quite widespread

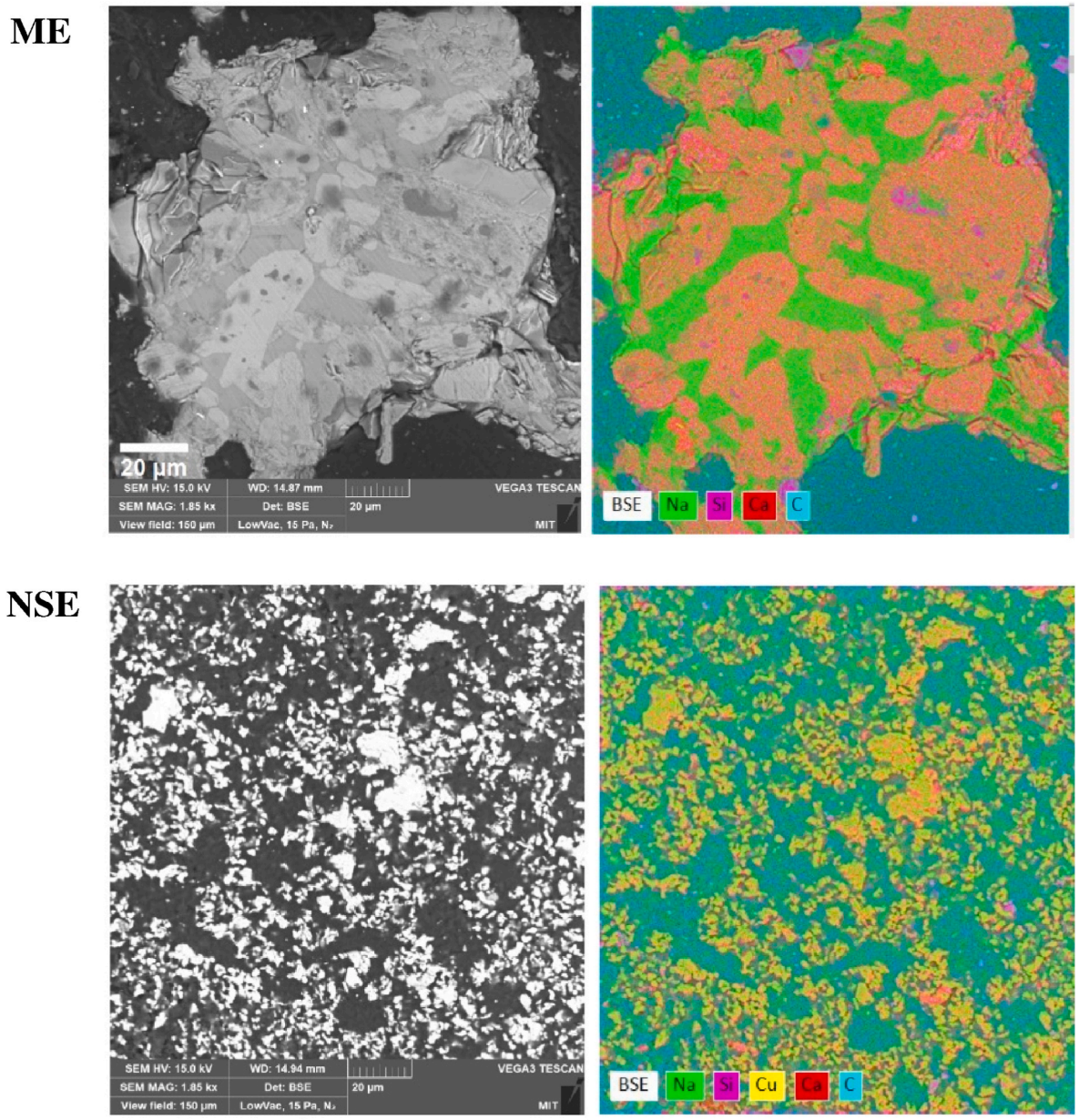

Fig. 3. SEM-BSE (left) and SEM-EDS (right) images of ME (top row) and NSE (bottom row) samples.

% for all the others (see Fig. 4). The samples exhibit a strong variability also in terms of absorbance in the NIR spectral region. In detail, in the spectral region around the emission peak (895–925 nm) the NSE sample has the lowest absorption coefficient (0.03 cm^{-1}), while samples prepared through the melt-flux method (ME, K120 and K10) have an absorbance value higher than 0.20 cm^{-1} (Fig. 4).

4. Discussion

Morphological and crystalline data demonstrate that EB synthesized starting from nanoparticles through innovative solid-state synthesis (NSE sample) is made of tiny cuprorivaite crystals (2–3 µm in diameter size) almost devoid of the glassy phase rich in copper and impurities, which is instead largely present in all EB samples synthesized with traditional melt-flux synthesis.

Optical data show that the PL of EB is greatly influenced by the route of synthesis and, in particular, by the presence and size of the glassy matrix surrounding cuprorivaite crystals. We speculate that the presence of a Cu-containing glass-matrix, formed as a result of melt-flux synthesis, is one of the main factors involved in a partial PL suppression. Indeed, by considering the higher NIR absorption coefficient measured for samples produced with a melt-flux method (ME, K120 and K10), it is possible to infer that the glassy matrix partially suppresses the cuprorivaite optical emission. This assessment can be explained by the chemical environment around Cu^{2+} when present in the glass-matrix that is different from that of Cu^{2+} in cuprorivaite. In crystalline cuprorivaite Cu^{2+} is in square-planar coordination and has specific absorptions at around 540, 625 and 780 nm, while in the glass-matrix Cu^{2+} can be present in a distorted octahedral site with a large optical absorption at longer wavelengths centered at 835 nm[64]. Therefore, this large absorption band, that partially overlaps with the optical emission of EB at around 915 nm, can decrease the actual emitted light because of auto-absorption or non-radiative energy transfer phenomena. This feature implies that a substantial decrease in EB luminescence can be produced because of increased vitrification (e.g. due to higher contents of fluxes or higher temperatures reached during synthesis).

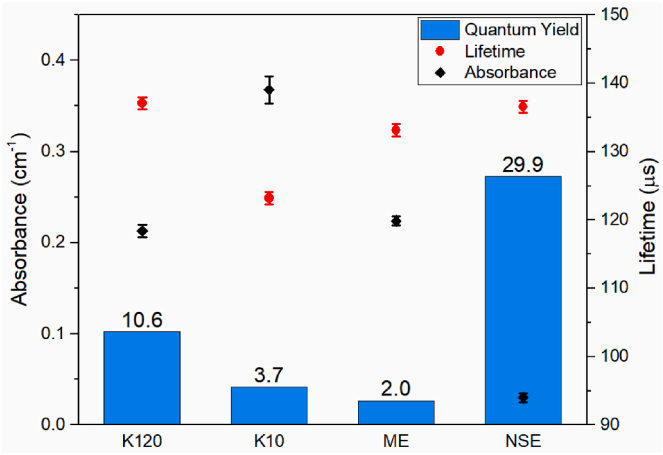

Fig. 4. Optical properties of K120, K10, ME, and NSE, provided as: PL quantum yield (cyan bar), PL lifetime (red diamonds) and absorption coefficient in the spectral region around EB emission peak (895–925 nm). (For interpretation of the references to color in this figure legend, the reader is referred to the Web version of this article.)

EB produced via solid-state synthesis shows a by far lower amount of amorphous structure and is thus preferable as a luminescent material. Nevertheless, as shown in Fig. 2, using commonly available micrometer grains of silica as a source of silicon for solid-state synthesis is a poor strategy. In fact, as observed for the SE sample, the formation of cuprorivaite is limited to the surface of the grains of silica, while the large part of the grain core stays unreacted. Instead, a better method to obtain EB with high quantum efficiency luminescence is starting from micrometer and submicrometer silica grains size or Synthetic Amorphous Silica (SAS) nanoparticles such as AEROSIL 200 (see also Patent application filed in Italy, number 102023000009153). The NSE sample obtained in this way displays superior emission features in comparison with EB obtained through other high-temperature synthesis routes and with commercial EBs that have been published as a high quantum-yield reference [7]. This enormous increase in quantum yield combined with the extremely high stability of EB in a wide range of temperature [21] and conditions and its high biocompatibility [4,5] can promote the replacement of luminescent materials based on toxic (i.e. CdS in Luminescent Solar Concentrators - LSC) or easily depleted materials (i.e. Rare Earth Elements REE in several applications such as near-infrared fluorophores for biomedical imaging) [27,31]. Indeed, such high efficiency in NIR phosphors is currently achievable using REE containing compounds such as SrF_2:Nd or LaF_3:Nd [65] or using fluorophores like modified boron dipyrromethenes (BODIPY) and others that, in general, can suffer of low photostability and/or biocompatibility issues [65,66].

An additional advantage of the NSE synthesis is that extensive grinding and milling are not required because the products are almost free from glass-matrix and made of smaller particles. In fact, it has to be noted that another aspect that can influence the luminescence output is the intensity of grinding. Heavy grinding has been considered responsible for a potential loss of luminescence due to the formation of defects, as expected for many phosphors [17]. An explanation could be that defects or changes in symmetry due to grinding enable non-radiative decay pathways or increase the radiative rate constants, as suggested in Selvaggio et al. [27] and noted in sample K10 in comparison with the unground K120 sample. While the aim of this research is to assess the impact of the route of synthesis, in the future more extensive work is needed to evaluate the impact of grinding and exfoliation on the luminescence output.

5. Conclusions

This work demonstrates that the quantum yield of EB can be modulated and improved using proper synthetic routes and has the potential to become even higher than the outstanding ca. 30 % recorded here (that is about 300 % higher than the one observed previously). The high quantum yield has important implications in the exploitation of EB in fields such as bioimaging, LSC and cool pigments. In particular, the mechanics described here can have a strong impact on the production of highly effective and sustainable new materials [8]. Indeed, EB is a highly sustainable material, with copper the only heavy metal present. Unlike many other fluorophores, its constituents are commonly available and safe, even in extensive applications such as bioimaging, cool pigments and LSC.

Finally, this work may impact the study of archaeological materials such as EB and closely related glassy materials, e.g. Egyptian green and blue Egyptian faience. In particular, the differences in PL due to degree of vitrification could be exploited to study ancient methods of production of the pigment, and as markers for the identification of ancient workshops or trade routes.

CRediT authorship contribution statement

Marco Nicola: Conceptualization, Methodology, Resources, Writing – original draft. **Claudio Garino:** Investigation, Validation, Writing – review & editing. **Sophia Mittman:** Investigation. **Emanuele Priola:** Investigation. **Luca Palin:** Investigation. **Marta Ghirardello:** Investigation, Visualization. **Vamshi Damagatla:** Investigation. **Austin Nevin:** Writing – review & editing. **Admir Masic:** Investigation. **Daniela Comelli:** Methodology, Validation, Writing – review & editing. **Roberto Gobetto:** Writing – review & editing, Supervision.

Declaration of competing interest

Nicola M., one of the authors of this paper, declares to be the inventor and to have partial ownership rights over the patent regarding the production of Egyptian blue from nanosilica. The patent is associated with Italy Patent Application Number 102023000009153, which has been filed. This competing interest does not in any way affect the objectivity, integrity, or impartiality of the research and its findings presented in this paper.

The other authors declare no competing interests with respect to the topic discussed.

Data availability

Data will be made available on request.

Acknowledgements

The authors would like to acknowledge funding from the European Union's Horizon 2020 Research and Innovation Programme as part of the PHAST-ETN project under the Marie Skłodowska-Curie Actions (Grant Agreement No. 860185)

Appendix A. Supplementary data

Supplementary data to this article can be found online at https://doi.org/10.1016/j.matchemphys.2023.128710.

References

[1] M. Nicola, R. Gobetto, A. Masic, Egyptian Blue , Chinese Blue , and Related Two - Dimensional Silicates : from Antiquity to Future Technologies . Part A : General Properties and Historical Uses, Springer International Publishing, 2023, https://doi.org/10.1007/s12210-023-01153-5.

[2] J. Jing, Y. Zhang, J. Sun, X. Zhao, D. Gao, Y. Zhang, A comparative study on different RE-doped (RE=Pr, Nd, Sm) SrCuSi4O10 blue pigments with high near-infrared reflectance, Dyes Pigments 150 (September 2017) (2018) 9–15, https://doi.org/10.1016/j.dyepig.2017.10.045.

[3] G. Pfaff, The world of inorganic pigments, ChemTexts 8 (3) (2022) 1–17, https://doi.org/10.1007/s40828-022-00166-1.

[4] T. Tian, C. Wu, J. Chang, Preparation and in vitro osteogenic, angiogenic and antibacterial properties of cuprorivaite (CaCuSi4O10, cup) bioceramics, RSC Adv. 6 (51) (2016) 45840–45849, https://doi.org/10.1039/C6RA08145B.

[5] C. He, C. Dong, L. Yu, Y. Chen, Y. Hao, Ultrathin 2D inorganic ancient pigment decorated 3D-printing scaffold enables photonic hyperthermia of osteosarcoma in NIR-II biowindow and concurrently augments bone regeneration, Adv. Sci. (2021) 1–10, https://doi.org/10.1002/advs.202101739, 2101739.

[6] P. Berdahl, S.K. Boocock, G.C.-Y. Chan, S.S. Chen, R.M. Levinson, M.A. Zalich, High quantum yield of the Egyptian blue family of infrared phosphors (MCuSi $_4$ O $_{10}$, M = Ca, Sr, Ba), J. Appl. Phys. 123 (19) (2018), 193103, https://doi.org/10.1063/1.5019808.

[7] G. Accorsi, G. Verri, M. Bolognesi, N. Armaroli, C. Clementi, C. Miliani, A. Romani, The exceptional near-infrared luminescence properties of cuprorivaite (Egyptian blue), Chem. Commun. 23 (2009) 3392, https://doi.org/10.1039/b902563d.

[8] G. Pozza, D. Ajò, G. Chiari, F. De Zuane, M. Favaro, Photoluminescence of the inorganic pigments Egyptian blue, han blue and han purple, J. Cult. Herit. 1 (4) (2000) 393–398, https://doi.org/10.1016/S1296-2074(00)01095-5.

[9] G. Verri, The spatially resolved characterisation of Egyptian blue, han blue and han purple by photo-induced luminescence digital imaging, Anal. Bioanal. Chem. 394 (4) (2009) 1011–1021, https://doi.org/10.1007/s00216-009-2693-0.

[10] J.A. Chaptal, Notice Sur Quelques Couleurs Trouvées à Pompéia, Ann. Chim. 70 (1) (1809) 22–31.

[11] Sir Humphry Davy, Some experiments and observations on the colours used in painting by the ancients, Philos. Trans. R. Soc. London, A 105 (1815) 97–124.

[12] J. Riederer, Egyptian blue, in: E.W. FitzHugh (Ed.), Artists' Pigments: A Handbook of Their History and Characteristics, vol. 3, National Gallery of Art, Washington, 1997, pp. 23–45.

[13] L. Bock, Über Ägyptischblau, in: E.W. FitzHugh (Ed.), Angew. Chem., vol. 29, National Gallery of Art, Washington, 1916, p. 228. ST-Egyptian blue.

[14] V. Daniels, R. Stacey, A. Middleton, The blackening of paint containing Egyptian blue, Stud. Conserv. 49 (4) (2004) 217–230, https://doi.org/10.2307/25487699.

[15] T.E. Warner, Artificial cuprorivaite CaCuSi4O10 (Egyptian blue) by a salt-flux method, in: Synthesis, Properties and Mineralogy of Important Inorganic Materials, Wiley, Chichester(UK), 2011, pp. 26–49, https://doi.org/10.1002/9780470976012.

[16] L. Binet, J. Lizion, S. Bertaina, D. Gourier, Magnetic and new optical properties in the UV–visible range of the Egyptian blue pigment cuprorivaite CaCuSi4O10, J. Phys. Chem. C (2021), https://doi.org/10.1021/acs.jpcc.1c06060.

[17] S.M. Borisov, C. Würth, U. Resch-Genger, I. Klimant, New life of ancient pigments: application in high-performance optical sensing materials, Anal. Chem. 85 (19) (2013) 9371–9377, https://doi.org/10.1021/ac402275g.

[18] P. Berdahl, S.K. Boocock, G.C.-Y. Chan, S.S. Chen, R.M. Levinson, M.A. Zalich, High quantum yield of the Egyptian blue family of infrared phosphors (MCuSi4O10 , M = Ca, Sr, Ba), J. Appl. Phys. 123 (19) (2018), 193103, https://doi.org/10.1063/1.5019808.

[19] S. Jose, D. Joshy, S.B. Narendranath, P. Periyat, Recent advances in infrared reflective inorganic pigments, Sol. Energy Mater. Sol. Cells 194 (September 2018) (2019) 7–27, https://doi.org/10.1016/j.solmat.2019.01.037.

[20] S. Jose, M.L. Reddy, Lanthanum-strontium copper silicates as intense blue inorganic pigments with high near-infrared reflectance, Dyes Pigments (2013), https://doi.org/10.1016/j.dyepig.2013.04.013.

[21] Y.-J. Li, S. Ye, C.-H. Wang, X.-M. Wang, Q.-Y. Zhang, Temperature-dependent near-infrared emission of highly concentrated Cu2+ in CaCuSi4O10 phosphor, J. Mater. Chem. C 2 (48) (2014) 10395–10402, https://doi.org/10.1039/C4TC01966K.

[22] B. Errington, G. Lawson, S.W. Lewis, G.D. Smith, Micronised Egyptian blue pigment: a novel near-infrared luminescent fingerprint dusting powder, Dyes Pigments 132 (2016) 310–315, https://doi.org/10.1016/j.dyepig.2016.05.008.

[23] P. Sobik, O. Jeremiasz, P. Nowak, A. Sala, B. Pawłowski, Towards efficient luminescent solar energy concentrator using cuprorivaite infrared phosphor (CaCuSi 4 O 10)— effect of dispersing method on photoluminescence intensity, Mater. MDPI 14 (3952) (2021), https://doi.org/10.3390/ma14143952.

[24] D. Johnson-McDaniel, T.T. Salguero, Exfoliation of Egyptian blue and han blue, two alkali earth copper silicate-based pigments, J. Vis. Exp. 3791 (86) (2014), https://doi.org/10.3791/51686.

[25] Y. Chen, M. Kan, Q. Sun, P. Jena, Structure and properties of Egyptian blue monolayer family: XCuSi4O10 (X = Ca, Sr, and Ba), J. Phys. Chem. Lett. (2016), https://doi.org/10.1021/acs.jpclett.5b02770.

[26] W. Chen, Y. Shi, Z. Chen, X. Sang, S. Zheng, X. Liu, J. Qiu, Near-infrared emission and Photon energy upconversion of two-dimensional copper silicates, J. Phys. Chem. C 119 (35) (2015) 20571–20577, https://doi.org/10.1021/acs.jpcc.5b04819.

[27] G. Selvaggio, M. Weitzel, N. Oleksiievets, T.A. Oswald, R. Nißler, I. Mey, V. Karius, J. Enderlein, R. Tsukanov, S. Kruss, Photophysical properties and fluorescence lifetime imaging of exfoliated near-infrared fluorescent silicate nanosheets, Nanoscale Adv. 3 (15) (2021) 4541–4553, https://doi.org/10.1039/d1na00238d.

[28] D. Johnson-Mcdaniel, C.A. Barrett, A. Sharafi, T.T. Salguero, Nanoscience of an ancient pigment, J. Am. Chem. Soc. 135 (5) (2012) 1677–1679, https://doi.org/10.1021/ja310587c.

[29] J. Petersen, J. Meruga, A. Baride, C. Bogart, W. Cross, S. May, J. Kellar, Visible-to-Infrared converting CaCuSi4O10 security ink, in: NIP & Digital Fabrication Conference, 2017, pp. 73–76.

[30] S.-S. Yang, H. Yu, Z. Wang, H.-L. Liu, X.-Z. Yu, W. Shang, G.-Q. Chen, Z.-Y. Gu, An exfoliated 2-D Egyptian blue nanosheet for highly selective enrichment of multi-phosphorylated peptides in mass spectrometric analysis, Chem. Eur J. 24 (9) (2017) 2109–2116, https://doi.org/10.1002/chem.201704138.

[31] G. Selvaggio, A. Chizhik, R. Nißler, D. Meyer, L. Vuong, H. Preiß, N. Herrmann, F. A. Mann, Z. Lv, T.A. Oswald, A. Spreinat, L. Erpenbeck, J. Großhans, V. Karius, A. Janshoff, J.P. Giraldo, S. Kruss, Exfoliated near infrared fluorescent silicate nanosheets for (Bio)Photonics, Nat. Commun. (2020) 1–11, https://doi.org/10.1038/s41467-020-15299-5.

[32] C. Yang, H. Ma, Z. Wang, M.R. Younis, C. Liu, 3D printed wesselsite nanosheets functionalized scaffold facilitates NIR-II photothermal therapy and vascularized bone regeneration, Adv. Sci. (2021) 1–11, https://doi.org/10.1002/advs.202100894, 2100894.

[33] C. Yang, R. Zheng, M.R. Younis, J. Shao, L.H. Fu, D.Y. Zhang, J. Lin, Z. Li, P. Huang, NIR-II light-responsive biodegradable shape memory composites based on cuprorivaite nanosheets for enhanced tissue reconstruction, Chem. Eng. J. 419 (November 2020) (2021), 129437, https://doi.org/10.1016/j.cej.2021.129437.

[34] P. García-Fernández, M. Moreno, J.A. Aramburu, Origin of the anomalous color of Egyptian and han blue historical pigments: going beyond the complex approximation in ligand field theory, J. Chem. Educ. 93 (1) (2016), https://doi.org/10.1021/acs.jchemed.5b00288.

[35] F. Mazzi, A. Pabst, Reexamination of cuprorivaite, Am. Mineral. 47 (1962) 409–411.

[36] A. Pabst, Structures of some tetragonal sheet silicates, Acta Crystallogr. 12 (1959) 733–739, https://doi.org/10.1107/S0365110X5900216X.

[37] E. Kendrick, C.J. Kirk, S.E. Dann, Structure and colour properties in the Egyptian blue family, M1-XM′xCuSi4O10, as a function of M, M′ where M, M′ = Ca, Sr and Ba, Dyes Pigments 73 (1) (2007) 13–18, https://doi.org/10.1016/j.dyepig.2005.10.006.

[38] T. Pradell, N. Salvado, G.D. Hatton, M.S. Tite, Physical processes involved in production of the ancient pigment, Egyptian blue, J. Am. Ceram. Soc. 89 (4) (2006) 1426–1431, https://doi.org/10.1111/j.1551-2916.2005.00904.x.

[39] A. Kiss, H.A. Stretz, A. Ueda, R. Mu, Synthesis of Egyptian blue and mechanisms, J. Phys. Chem. Solid. (2022), 138954, https://doi.org/10.1016/j.jpcs.2022.110738.

[40] A. Kiss, Enhanced Near-Infrared Emission in Supramarble Coatings of Egyptian Blue, Tennessee Technological University, 2023.

[41] F. Delamare, Sur Les Processus Physiques Intervenant Lors de La Synthèse Du Bleu Égyptien : Réflexion à Propos de La Composition de Pigments Bleux Gallo-Romains, Rev. d'Archéométrie 21 (1997) 103–119.

[42] M. Nicola, L.M. Seymour, M. Aceto, E. Priola, R. Gobetto, A. Masic, Late production of Egyptian blue: synthesis from brass and its characteristics, Archaeol. Anthropol. Sci. 11 (10) (2019) 5377–5392, https://doi.org/10.1007/s12520-019-00873-w.

[43] M.P. Etcheverry, M. Schvoerer, F. Bechtel, Bleu égyptien: mise en évidence de Deux processus de Formation de La cuprorivaïte, Rev. d'Archéométrie 25 (2001) 87–100.

[44] D. Johnson-McDaniel, S. Comer, J.W. Kolis, T.T. Salguero, Hydrothermal Formation of calcium copper tetrasilicate, Chem. Eur J. 21 (49) (2015) 17560–17564, https://doi.org/10.1002/chem.201503364.

[45] A. Panagopoulou, K. Karanasios, G. Xanthopoulou, Ancient Egyptian blue (CaCuSi4O10) pigment by modern solution combustion synthesis method, Eurasian Chem. J. 18 (1) (2016) 31–37, https://doi.org/10.18321/ectj390.

[46] Y. Zhang, Y. Zhang, X. Zhao, Y. Zhang, Sol-gel synthesis and properties of europium-strontium copper silicates blue pigments with high near-infrared reflectance, Dyes Pigments 131 (2016) 154–159, https://doi.org/10.1016/j.dyepig.2016.04.011.

[47] P. Loch, T. Martin, M. Grüner, G. Kaupp, W. Schwieger, J. Breu, Synthesis of large platelets of Egyptian blue via pseudomorphosis after NaRUB-18, Zeitschrift fur Anorg. und Allg. Chem. 646 (18) (2020) 1570–1574, https://doi.org/10.1002/zaac.202000203.

[48] R.S.P. King, P.M. Hallett, D. Foster, NIR–NIR fluorescence: a new genre of fingermark visualisation techniques, Forensic Sci. Int. 262 (2016) e28–e33.

[49] T. Rajaramanan, M. Keykhaei, F.H. Gourji, et al., Eco-friendly Egyptian blue (CaCuSi4O10) dye for luminescent solar concentrator applications, Mater. Adv. (2023), https://doi.org/10.1039/d2ma01106a.

[50] Y. Zhuang, S. Tanabe, Forward and back energy transfer between Cu2+ and Yb3+ in Ca1-XCuSi4O10:ybx crystals, 0–6, J. Appl. Phys. 112 (9) (2012), https://doi.org/10.1063/1.4765013.

[51] M. Nicola, Ancient Materials Inspiring New Technologies: the Egyptian Blue, Università di Torino, 2019.

[52] A. Kiss, H.A. Stretz, Egyptian Blue/gold nanocomposite supramarbles, a platform for IR emission enhancement, Mater. Chem. Phys. 309 (2023), 128329, https://doi.org/10.1016/j.matchemphys.2023.128329.

[53] R. Linn, D. Comelli, G. Valentini, S. Mosca, A. Nevin, Egyptian blue pigment in east mediterranean wall paintings: a study of the lifetime of its optical infrared emission, Strain (April) (2018), e12277, https://doi.org/10.1111/str.12277.

[54] M. Godet, L. Binet, S. Schoder, M. Thoury, L. Bertrand, X-ray irradiation effects on Egyptian blue and green pigments, J. Anal. At. Spectrom. (2022), https://doi.org/10.1039/d2ja00020b.

[55] Y. Cai, W. Peng, Q. Song, D. Pluta, C. Peppersack, S. Breitung-faes, A. Kwade, N. C. Bigall, P. Vana, Nanoengineering of Egyptian blue nanosheets: advantages and limitations for near-infrared photoluminescence applications, ACS Appl. Opt. Mater. (2022), https://doi.org/10.1021/acsaom.2c00114.

[56] S. Shahbazi, J.V. Goodpaster, G.D. Smith, T. Becker, S.W. Lewis, Preparation, characterization, and application of a lipophilic coated exfoliated Egyptian blue for near-infrared luminescent latent fingermark detection, Forensic Chem. 18 (2020), 100208, https://doi.org/10.1016/j.forc.2019.100208.

[57] V.A. Yuryev, T.V. Yuryeva, I.F. Kadikova, S.A. Malykhin, A.A. Klimenko, K. V. Chizh, Photoluminescence and cathodoluminescence of CaCu(Si2O5)2, SSRN Electron. J. (2023), https://doi.org/10.2139/ssrn.4362577.
[58] B. Hill, S. Abraham, A. Akhtar, G. Selvaggio, K. Tschulik, S. Kruss, Surfactant assisted exfoliation of near infrared fluorescent silicate nanosheets, RSC Adv. (2023) 20916–20925, https://doi.org/10.1039/d3ra04083f.
[59] L.D. Mitchell, J.C. Margeson, P.S. Whitfield, Quantitative Rietveld analysis of hydrated cementitious systems, Powder Diffr. 21 (2) (2006) 111–113, https://doi.org/10.1154/1.2204056.
[60] A.A. Coelho, TOPAS and TOPAS-academic : an optimization program integrating computer algebra and crystallographic objects written in C++, J. Appl. Crystallogr. 51 (1) (2018) 210–218, https://doi.org/10.1107/S1600576718000183.
[61] www.topas-academic.net.
[62] S. Bellei, A. Nevin, A. Cesaratto, V. Capogrosso, H. Vezin, C. Tokarski, G. Valentini, D. Comelli, Multianalytical study of historical luminescent lithopone for the detection of impurities and trace metal ions, Anal. Chem. 87 (12) (2015) 6049–6056, https://doi.org/10.1021/acs.analchem.5b00560.
[63] C. D'Andrea, E.A. Obraztsova, A. Farina, P. Taroni, G. Lanzani, A. Pifferi, Absorption spectroscopy of powdered materials using time-resolved diffuse optical methods, Appl. Opt. 51 (32) (2012) 7858, https://doi.org/10.1364/AO.51.007858.
[64] S. Pagès-Camagna, I. Reiche, C. Brouder, D. Cabaret, S. Rossano, B. Kanngießer, A. Erko, New insights into the colour origin of archaeological Egyptian blue and green by XAFS at the Cu K-edge, X Ray Spectrom. 35 (2) (2006) 141–145, https://doi.org/10.1002/xrs.885.
[65] G. Hong, A.L. Antaris, H. Dai, Near-infrared fluorophores for biomedical imaging, Nat. Biomed. Eng. 1 (10) (2017) 1–22, https://doi.org/10.1038/s41551-016-0010.
[66] G. Selvaggio, S. Kruss, Preparation, properties and applications of near-infrared fluorescent silicate nanosheets, Nanoscale 14 (2022) 9553–9575, https://doi.org/10.1039/d2nr02967g.